# Reggeized Deck model for $\pi^- p \to \rho^0 \pi^- p$ obeying the Steinmann relation

Michael J. Puhala
*Department of Physics, University of Illinois at Urbana-Champaign, Urbana, Illinois 61801*
(Received 22 July 1977)

We construct a Reggeized Deck model for the reaction $\pi^- p \to \pi^+ \pi^- \pi^- p$ that satisfies the Steinmann relation in the physical region. The $\rho$-$\pi$ mass spectrum is reproduced with a slightly improved width, and the $\rho$-$\pi$ partial waves agree with the results of previous calculations. An explanation for the success of the Reggeization in this low-$\rho\pi$-mass region is given. Resonancelike behavior is isolated in the $\rho$-$\pi$–cut term, and a resonance-type loop is shown to be present in the $1^+ s$-wave Argand diagram. The difficulty associated with observing a hypothetical $A_1$ meson in this reaction is discussed.

## I. INTRODUCTION

A series of calculations[1,2] using a Reggeized Deck model has reproduced quite well the experimentally determined phases of the $3\pi$ partial waves in the reaction $\pi^- p \to \pi^+ \pi^- \pi^- p$. This model suffered from the defect of violating the Steinmann relation.[3-5] The Steinmann relation forbids the presence of simultaneous discontinuities in overlapping energy variables in an amplitude for a scattering process, provided that the discontinuities are taken in the physical region of the scattering process. A recent paper by Jones[6] considered only quasi-three-body final states like $\rho^0 \pi^- p$, and demonstrated that if the double-Regge residue obeyed a particular constraint at $t_{\text{proton}} \approx 0$, pronounced cancellations occurred, and the standard Mellin representation[7] for the five-particle amplitude approximates the successful "naive" model at this point.

In this paper, we assume that the reaction proceeds entirely via

$$\pi^- p \to \rho^0 \pi^- p \quad (\rho^0 \to \pi^+ \pi^-).$$

We shall continue Jones's work and obtain a double-Regge residue, valid for a range of momentum transfers, that satisfies the mentioned constraint for $t_{\text{proton}} \approx 0$. In Sec. II we demonstrate that the form of the "constrained" residue is largely determined for arbitrary momentum transfer by the known analytic structure of the amplitude. The amplitude that we obtain may be neatly expressed in terms of hypergeometric functions which explicitly display the correct discontinuity structure in the physical region of the reaction.

In Sec. III we give various kinematic formulas. We also give the expressions used to calculate the partial wave amplitudes.

In Sec. IV we discuss the resulting $\rho$-$\pi$ mass spectrum and other distributions. The behavior of several partial waves is displayed. We find that the width of the $A_1$ bump is slightly improved, and the behavior of the partial waves is similar to that obtained by Ascoli *et al.*

In Sec. V we consider the contributions of the separate terms with distinct cut structures. It is found that the term with the cut in the outgoing pion-proton subenergy dominates. An explanation for the success of Reggeization in this reaction is given. We partial-wave-analyze the separate terms and show that the term with the cut in the $\rho$-$\pi$ subenergy acts as though it contains the entire resonant behavior of the amplitude. A description of how a hypothetical $A_1$ "meson" could be hidden in the partial-wave data is also presented.

Finally, in Sec. VI we present a summary of the main results.

## II. THE MODEL

Our labeling of kinematics for the reaction $\pi^- p \to \rho^0 \pi^- p$ is shown in Fig. 1. The momenta $p_1$ and $p_2$ are those of the incident pion and proton, respectively; $q_1$, $q$, and $q_2$ are the momenta of the outgoing $\rho$, pion, and proton. Our overcomplete set of kinematic invariants is given by

$$\begin{aligned} s_{12} &= (p_1 + p_2)^2, \\ s_1 &= (q_1 + q)^2, \\ s_2 &= (q_2 + q)^2, \\ t_1 &= (p_1 - q_1)^2, \\ t_2 &= (p_2 - q_2)^2, \\ \eta &= \frac{s_{12}}{s_1 s_2}, \\ M_{\rho\pi} &= \sqrt{s_1}. \end{aligned} \tag{2.1}$$

Following others,[1,8] we omit the proton helicities completely, and take the $t_1$-channel helicity amplitude with the $\rho$ having zero helicity to be the sole contributor to the cross section. We may then

write the familiar[9] Mellin representation for the signatured double-Regge amplitude:

$$A_5^{\tau_1\tau_2} = \frac{\beta_1(t_1)\beta_2(t_2)}{2\pi i} \times \int d\lambda\, \Gamma(-\lambda)\Gamma(\lambda-\alpha_1)\Gamma(\lambda-\alpha_2)(-s_1)^{\alpha_1-\lambda} \times (-s_2)^{\alpha_2-\lambda}(-s_{12})^{\lambda}\beta(\lambda;t_1,t_2)\,. \quad (2.2)$$

In the above, $\alpha_1$ and $\alpha_2$ are the $\pi$ and Pomeron trajectories, respectively. The variable $\lambda$ is to leading order the complex helicity of the two Reggeons. It has been shown by Jones[6] that the above will reduce to an amplitude with the phase of the "naive" Deck model[2] if the double-Regge residue $\beta(\lambda;t_1,t_2)$ obeys the following constraint at $t_2=0$:

$$\beta(\lambda;t_1,0) = \frac{(1-\lambda)}{\Gamma(\lambda+1)\eta^{\lambda}}\beta(0;t_1,0)\,. \quad (2.3)$$

We first observe that for an event in which the proton is forward scattered in the center-of-mass frame of the initial state, if we fix the values of $s_{12}$ and $s_1$, we necessarily specify $s_2$. Its value is given by

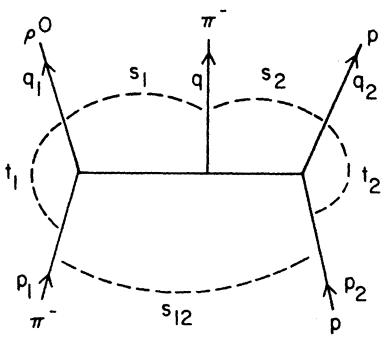


FIG. 1. Kinematics for the double-Regge exchange considered in the text.

$$s_{2\,\text{forward proton}} = s_{12} + m_\rho^2 + 2\frac{(s_1+m_\rho^2-m_\pi^2)\lambda^{1/2}(s_{12},m_\pi^2,m_N^2) - (m_\pi^2+m_\rho^2-t_1)\lambda^{1/2}(s_{12},s_1,m_N^2)}{(s_{12}+m_\pi^2-m_N^2)\lambda^{1/2}(s_{12},s_1,m_N^2) - \lambda^{1/2}(s_{12},m_\pi^2,m_N^2)(s_{12}+s_1-m_N^2)}\,, \quad (2.4)$$

where $\lambda(a,b,c) = a^2+b^2+c^2-2ab-2ac-2bc$. It follows that $\eta$ is uniquely determined in this case, depending only on $s_{12}$, $s_1$, and $t_1$. In the double-Regge limit, i.e., $s_1, s_2, s_{12} \to \infty, t_1, t_2, \eta$ fixed, we have to leading order

$$\eta_{\text{forward}} = (m_\pi^2 - t_1)^{-1}\,. \quad (2.5)$$

The corresponding value of $t_2$ we will denote by $t_{2M}$, where

$$t_{2M} = 2m_N^2 - \frac{(s_{12}+m_N^2-m_\pi^2)(s_{12}+m_N^2-s_1)}{2s_{12}} + \frac{\lambda^{1/2}(s_{12},m_N^2,m_\pi^2)\lambda^{1/2}(s_{12},m_N^2,s_1)}{2s_{12}}\,. \quad (2.6)$$

To leading order, we have $t_{2M} = -(s_1-m_\pi^2)^2 m_N^2/2(s_{12})^2$. In the double-Regge limit, we have $t_{2M} \to 0$. In this limit, Eq. (2.3) will be satisfied by a function of the following form:

$$\beta(\lambda;t_1,t_2) = \frac{(1-\lambda)P(t_1,t_2)}{\Gamma(\lambda+1)M(t_1,t_2)^{\lambda}}\,. \quad (2.7)$$

We shall show that the function $M(t_1,t_2)$ is largely determined by the analytic structure of the amplitude in the $s_{12}$ channel, and Eq. (2.3). In addition, the function $P(t_1,t_2)$ will be related to single-Regge residues obtained from two-body reactions by examining the pion pole term in the $t_1$ channel.

In order to determine $M(t_1,t_2)$, we first note that by Eq. (2.3) it is subject to the constraint $M(t_1,0) = \eta$. In the double-Regge limit, we may instead impose the condition

$$M(t_1,t_{2M}) = \eta\,. \quad (2.8)$$

We now recall the familiar integral representation of the hypergeometric function:

$$F(a,b|c|z) = \frac{\Gamma(c)}{\Gamma(a)\Gamma(b)}\int_{-i\infty}^{+i\infty}\frac{\Gamma(a+t)\Gamma(b+t)}{2\pi i\Gamma(c+t)} \times \Gamma(-t)(-z)^t\,dt\,. \quad (2.9)$$

If we substitute Eq. (2.7) into Eq. (2.2), we obtain

$$A_5^{\tau_1\tau_2} = \beta_1(t_1)\beta_2(t_2)P(t_1,t_2)(-s_1)^{\alpha_1}(-s_2)^{\alpha_2}\Gamma(-\alpha_1)\Gamma(-\alpha_2)[F(-\alpha_1,-\alpha_2|1|\eta/M) - \alpha_1\alpha_2(\eta/M)F(1-\alpha_1,1-\alpha_2|2|\eta/M)]\,. \quad (2.10)$$

In the above, we have written $M(t_1,t_2) = M$. On examination of the hypergeometric series

$$F(a,b|c|z) = \frac{\Gamma(c)}{\Gamma(a)\Gamma(b)}\sum_{n=0}^{\infty}\frac{\Gamma(a+n)\Gamma(b+n)}{n!\,\Gamma(c+n)}\,z^n \quad (2.11)$$

we see that the hypergeometric functions appearing in Eq. (2.10) are analytic for $0 \leq \eta/M < 1$. This is undesirable, for the factor $(-s_1)^{\alpha_1}(-s_2)^{\alpha_2}$ will yield simultaneous discontinuities in the channel subenergies $s_1$ and $s_2$, violating the Steinmann relations.[3-5,7,9] Therefore, the amplitude will have an improper discontinuity structure in the physical region of the reaction unless $\eta/M \geq 1$.

We may use another well-known relation among the hypergeometric functions,

$$\frac{\Gamma(a)\Gamma(b)}{\Gamma(c)} F(a,b|c|z) = \frac{\Gamma(a)\Gamma(b-a)}{\Gamma(c-a)} (-z)^{-a} F(a, 1-c+a|1-b+a|1/z) + \frac{\Gamma(b)\Gamma(a-b)}{\Gamma(c-b)} (-z)^{-b} F(b, 1-c+a|1-a+b|1/z) . \tag{2.12}$$

to rewrite the amplitude in the following form:

$$A_5^{\tau_1\tau_2} = \beta_1(t_1)\beta_2(t_2)(-s_1)^{\alpha_1}(-s_2)^{\alpha_2}\Gamma(-\alpha_1)\Gamma(-\alpha_2)[(-\eta)^{\alpha_1}V_1(t_1,t_2;\eta) + (-\eta)^{\alpha_2}V(t_1,t_2;\eta)] . \tag{2.13}$$

The double-Regge vertices $V_1(t_1,t_2;\eta), V_2(t_1,t_2;\eta)$, are given by

$$V_1(t_1,t_2;\eta) = \frac{P(t_1,t_2)}{M(t_1,t_2)^{\alpha_1}} \frac{\Gamma(\alpha_2-\alpha_1)}{\Gamma(1+\alpha_1)} [F(-\alpha_1,-\alpha_1|1-\alpha_1+\alpha_2|M/\eta) - \alpha_1 F(1-\alpha_1,-\alpha_1|1-\alpha_1+\alpha_2|M/\eta)] , \tag{2.14}$$

$$V_2(t_1,t_2;\eta) = \frac{P(t_1,t_2)}{M(t_1,t_2)^{\alpha_2}} \frac{\Gamma(\alpha_1-\alpha_2)}{\Gamma(1+\alpha_2)} [F(-\alpha_2,-\alpha_2|1-\alpha_2+\alpha_1|M/\eta) - \alpha_2 F(1-\alpha_2,-\alpha_2|1-\alpha_2+\alpha_1|M/\eta)] . \tag{2.15}$$

If we choose $M(t_1,t_2)$ such that $M/\eta \leq 1$ in the physical region, then $V_1(t_1,t_2;\eta)$ and $V_2(t_1,t_2;\eta)$ are both real in the physical region of the reaction. The hypergeometric functions are finite at $M/\eta = 1$ if $\alpha_1+\alpha_2 \geq 0$, which is certainly true for $t_1, t_2$ small. The factors $(-\eta)^{\alpha_1}$ and $(-\eta)^{\alpha_2}$ nicely cancel the unwanted simultaneous discontinuities. A function which satisfies the condition $M/\eta \leq 1$ and Eq. (2.8) is given by

$$M(t_1,t_2) = \frac{s_{12}}{s_1 s_{2\,\max}(s_{12},s_1,t_1,t_2)} . \tag{2.16}$$

In the above, $s_{2\,\max}$ is the maximum value of $s_2$ kinematically permitted, given $s_{12}$, $s_1$, $t_1$, and $t_2$. If we denote the rest frame of the $\rho$-$\pi$ final state by the superscript $M$ (see Fig. 2), we may write

$$s_{2\max} = m_N^2 + m_\pi^2 + 2q_{20}^M q_0^M + 2|\vec{q}_2^{\,M}||\vec{q}^{\,M}|(\cos\theta_1\cos\psi_2 + \sin\theta_1\sin\psi_2) , \tag{2.17}$$

where $q_{20}^M$ and $q_0^M$ are the energies of the outgoing proton and pion, respectively, in the $\rho$-$\pi$ rest frame [see Eq. (3.2)]. The angle $\theta_1$ is the angle between the incident $\pi$ and the outgoing $\rho$ in the $M$ frame, and $\psi_2$ is the angle between the incident $\pi$ and outgoing proton, also measured in the $M$ frame.

We see that Eq. (2.17) contains $s_{12}$ and $s_1$ dependence. Its leading-order expansion, however, is given by

$$s_{2\,\max}(s_{12},s_1,t_1,t_2) = \frac{s_{12}}{s_1}[m_\pi^2 - t_1 - t_2 + 2(t_1t_2)^{1/2}] + O(s_{12}^{\,0}, s_1^{\,-2}) . \tag{2.18}$$

To leading order then,

$$M(t_1,t_2) = [m_\pi^2 - t_1 - t_2 + 2(t_1t_2)^{1/2}]^{-1} + O\left(\frac{1}{s_{12}}, \frac{1}{s_1}\right) . \tag{2.19}$$

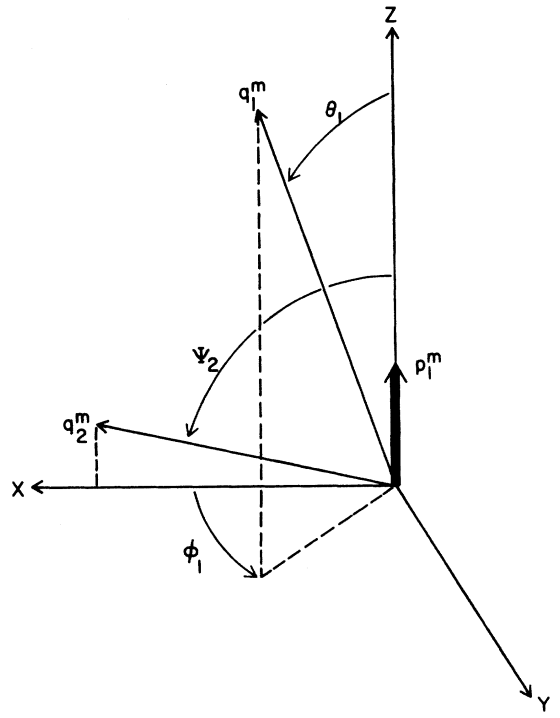


FIG. 2. Orientation of the $M$ frame ($\rho$-$\pi$ rest frame).

In the double-Regge limit, the dependence on $s_{12}$ and $s_1$ disappears; as a result $M(t_1, t_2)$ depends only on $t_1$ and $t_2$. It should be noted that the factor $(t_1 t_2)^{1/2}$ contains simultaneous discontinuities in $t_1$ and $t_2$. Since these channels do not overlap, this is, in fact, permissible. A more serious objection is that the term $(t_1 t_2)^{1/2} = (-t_1)^{1/2}(-t_2)^{1/2}$ yields simultaneous discontinuities in $s_1$ and $t_1$, $s_2$ and $t_2$, $s_{12}$ and $t_1$, etc.; these unwanted discontinuities occur, however, only for $t_1 > 0$ or $t_2 > 0$. Since these unwanted cuts do not appear in our model in the physical region of the reaction that we are studying, we shall regard our choice of $M(t_1, t_2)$ to be an "adequate" parametrization of the "true" function in the physical region. In particular, it yields the correct combination of signature factors in the full amplitude, thus assuring that the amplitude has the correct phase in the physical region.

It should also be noted that the choice given in Eq. (2.16) is not entirely unique; for example, we could also consider the function

$$M'(t_1, t_2) = \frac{s_{12}}{s_2 s_{1\max}(s_{12}, s_2, t_1, t_2)} , \tag{2.20}$$

where $s_{1\max}(s_{12}, s_2, t_1, t_2)$ is the maximum value of $s_1$ kinematically permitted, given $s_{12}$, $s_2$, $t_1$, and $t_2$. To leading order, we have

$$M'(t_1, t_2) = [m_\pi^2 - t_1 - t_2 + 2(t_1 t_2)^{1/2}]^{-1} + O\left(\frac{1}{s_{12}}, \frac{1}{s_2}\right) . \tag{2.21}$$

Therefore, $M(t_1, t_2)$ and $M'(t_1, t_2)$ differ in nonleading terms. We shall use the choice $M(t_1, t_2)$ and later comment on its appropriateness.

We now will determine the function $P(t_1, t_2)$, and obtain a result independent of our choice of $M(t_1, t_2)$. We first consider the full amplitude, obtained by summing over all the allowed cuts,[10] and obtain

$$A_5 = \beta_1(t_1) s_1^{\alpha_1} \Gamma(-\alpha_1) \beta_2(t_2) s_2^{\alpha_2} \Gamma(-\alpha_2) \times [\xi_1 \xi_{21} \eta^{\alpha_1} V_1(t_1, t_2; \eta) + \xi_2 \xi_{12} \eta^{\alpha_2} V_2(t_1, t_2; \eta)] . \tag{2.22}$$

The signature factors are given by

$$\xi_i = e^{-i\pi\alpha_i} + 1 , \qquad \xi_{ij} = e^{-i\pi(\alpha_i - \alpha_j)} + 1 . \tag{2.23}$$

We shall wish to compare the above with the "exact" $t_1$-channel helicity amplitude corresponding to a $\rho$ meson with helicity $\mu$, which we denote by $f_\mu^{(t_1)}$. Following Berger,[11] we write down the $\mu = 0$ amplitude near $t_1 = m_\pi^2$; from unitarity, the pion pole dominates, and we have

$$f_0^{(t_1)} \approx -g_{\rho\pi\pi}(m_\rho^2 - 4m_\pi^2)^{1/2} \frac{M_{\pi p \to \pi p}}{t_1 - m_\pi^2 + i\epsilon} . \tag{2.24}$$

In the above, $g_{\rho\pi\pi}$ is the effective $\rho\pi\pi$ coupling constant. It is real and positive with $g_{\rho\pi\pi}^2/4\pi = 2.2$. The quantity $M_{\pi p \to \pi p}$ is the on-mass-shell elastic $\pi$-$p$ scattering amplitude (neglecting proton helicities) for a center-of-mass energy $s_2$ and momentum transfer $t_2$. For the purposes of our analysis we use the Reggeized form

$$M_{\pi p \to \pi p} = \beta_{\pi P \pi}(t_2) \beta_{NPN}(t_2) \xi_2 \Gamma(-\alpha_2) s_2^{\alpha_2} , \tag{2.25}$$

where the residues $\beta_{\pi P \pi}(t_2), \beta_{NPN}(t_2)$ give the coupling of the Pomeron to the pion and proton, respectively.

We now wish to evaluate the residue of $A_5$ at $t_1 = m_\pi^2$. The pole expansions[9] for the double-Regge vertices are given by

$$V_1(t_1, t_2; \eta) = \frac{1}{\Gamma(-\alpha_1)\Gamma(-\alpha_2)} \sum_{n=0}^{\infty} \frac{1}{n!} \Gamma(n - \alpha_1)\Gamma(\alpha_1 - \alpha_2 - n)\eta^{-n} \beta(\alpha_1 - n; t_1, t_2) , \tag{2.26}$$

$$V_2(t_1, t_2; \eta) = \frac{1}{\Gamma(-\alpha_1)\Gamma(-\alpha_2)} \sum_{n=0}^{\infty} \frac{1}{n!} \Gamma(n - \alpha_2)\Gamma(\alpha_2 - \alpha_1 - n)\eta^{-n} \beta(\alpha_2 - n; t_1, t_2) . \tag{2.27}$$

We compute the following residues at the pion pole, where $\alpha_1 = 0$, $d\alpha_1/dt_1 = 1$:

$$\mathrm{Res}\{\Gamma(-\alpha_1)\Gamma(-\alpha_2) V_1(t_1, t_2; \eta)\}|_{t_1 = m_\pi^2} = -\Gamma(-\alpha_2) P(m_\pi^2, t_2) , \tag{2.28}$$

$$\mathrm{Res}\{\Gamma(-\alpha_1)\Gamma(-\alpha_2) V_2(t_1, t_2; \eta)\}|_{t_1 = m_\pi^2} = 0 .$$

From Eq. (2.22), we get that

$$\mathrm{Res} A_5|_{t_1 = m_\pi^2} = -2\beta_1(m_\pi^2)\beta_2(t_2) s_2^{\alpha_2} \xi_2 \times \Gamma(-\alpha_2) P(m_\pi^2, t_2) . \tag{2.29}$$

As we have previously suggested, the above is independent of $M(t_1, t_2)$. If we set $\mathrm{Res} f_0^{(t_1)}|_{t_1 = m_\pi^2} = \mathrm{Res} A^5|_{t_1 = m_\pi^2}$, after cancelling some common factors we obtain

$$\beta_1(m^2)\beta_2(t_2) 2P(m_\pi^2, t_2) = g_{\rho\pi\pi}(m_\rho^2 - 4m_\pi^2)^{1/2} \beta_{\pi P \pi}(t_2) \beta_{NPN}(t_2) . \tag{2.30}$$

Now White has demonstrated[12] the factorization of the single-Regge couplings in the five-particle amplitude; hence we may write

$$\beta_2(t_2)=\beta_{NPN}(t_2)\,. \tag{2.31}$$

In the spirit of previous work[1,8,11] we assume a constant $\rho\pi\pi$ coupling; factorization then permits us to write

$$\beta_1(t_1)=g_{\rho\pi\pi}(m_\rho{}^2-4m_\pi{}^2)^{1/2}\,. \tag{2.32}$$

From Eq. (2.30) we conclude that

$$P(t_1,t_2)=\tfrac{1}{2}\beta_{\pi P\pi}(t_2)\,. \tag{2.33}$$

To complete our specification of the model, we used a curved trajectory of the Pignotti type

$$\alpha_1=-(m_\pi{}^2-t_1)/(m_\pi{}^2-t_1+1) \tag{2.34}$$

and a moving Pomeron trajectory

$$\alpha_2=1.0+0.275t_2\,. \tag{2.35}$$

The choice

$$\beta_{\pi P\pi}(t_2)\beta_{NPN}(t_2)=Ce^{bt_2} \tag{2.36}$$

with $2b=6.75$ yields a $\pi^-p$ differential cross section proportional to $\exp(8t_2)$ at $s_2=10$ (GeV)$^2$. From the optical theorem we may write

$$C=\sigma_{\pi N}/\pi\,, \tag{2.37}$$

where $\sigma_{\pi N}$ is the $\pi^-p$ total cross section $\sigma_{\pi N}=29$ mb.

As a matter of calculational convenience, the double-Regge vertices may be rewritten as a power series in $1-M/\eta$, namely

$$V_1(t_1,t_2;\eta)=\frac{P(t_1,t_2)\pi M(t_1,t_2)^{-\alpha_1}}{\sin\pi(\alpha_1-\alpha_2)\Gamma(1+\alpha_2)}$$

$$\times\left\{\frac{\Gamma(\alpha_1+\alpha_2)}{\Gamma(1+\alpha_1)^2}\left[(\alpha_1+\alpha_2)F(-\alpha_2,-\alpha_2|-\alpha_1-\alpha_2|1-M/\eta)\right.\right.$$

$$\left.-\alpha_1\alpha_2F(1-\alpha_2,-\alpha_2|1-\alpha_1-\alpha_2|1-M/\eta)\right]$$

$$-\frac{\Gamma(-\alpha_1-\alpha_2)}{\Gamma(-\alpha_2)^2}(1-M/\eta)^{\alpha_1+\alpha_2}\left[(1-M/\eta)\frac{F(1+\alpha_1,1+\alpha_1|2+\alpha_1+\alpha_2|1-M/\eta)}{1+\alpha_1+\alpha_2}\right.$$

$$\left.\left.-F(\alpha_1,1+\alpha_1|1+\alpha_1+\alpha_2|1-M/\eta)\right]\right\}\,. \tag{2.38}$$

The corresponding expansion for $V_2(t_1,t_2;\eta)$ may be obtained by interchanging $\alpha_1$ and $\alpha_2$. These forms have the practical advantage that since $[M(t_1,t_2)]/\eta$ is near 1 in the regions of phase space that contribute most heavily to the cross section, the resulting hypergeometric series are easy to evaluate.

## III. PARTIAL-WAVE FORMULAS

We shall find it interesting to determine the partial-wave content of our amplitude, in hope of observing resonancelike behavior, or its absence.[1,8] Following Ascoli *et al.*,[1] we define our coordinate system as in Fig. 2. Vectors in the $M$ frame are denoted by the superscript $M$. The $M$ frame is defined by the condition $\vec{q}_1^{\,M}+\vec{q}^{\,M}=0$, and the orientation

$$\begin{aligned}
&p_1^M=(p_{10}^M,0,0,|\vec{p}_1^{\,M}|)\,,\\
&q_2^M=(q_{20}^M,|\vec{q}_2^{\,M}|\sin\psi_2,0,|\vec{q}_2^{\,M}|\cos\psi_2)\,,\\
&q_1^M=(q_{10}^M,|\vec{q}_1^{\,M}|\sin\theta_1\cos\phi_1,|\vec{q}_1^{\,M}|\sin\theta_1\sin\phi_1,|\vec{q}_1^{\,M}|\cos\theta_1)\,.
\end{aligned} \tag{3.1}$$

In terms of our set of invariant quantities, the above are given by

$$\begin{aligned}
&p_{10}^M=\frac{m_\pi{}^2+s_1-t_2}{2\sqrt{s_1}}\,,\quad |\vec{p}_1^{\,M}|=\frac{\lambda^{1/2}(m_\pi{}^2,s_1,t_2)}{2\sqrt{s_1}}\,,\\
&q_{20}^M=\frac{s_{12}-m_N{}^2-s_1}{2\sqrt{s_1}}\,,\quad |\vec{q}_2^{\,M}|=\frac{\lambda^{1/2}(s_{12},m_N{}^2,s_1)}{2\sqrt{s_1}}\,,\\
&q_{10}^M=\frac{s_1+m_\rho{}^2-m_\pi{}^2}{2\sqrt{s_1}}\,,\quad |\vec{q}_1^{\,M}|=\frac{\lambda^{1/2}(s_1,m_\rho{}^2,m_\pi{}^2)}{2\sqrt{s_1}}\,,\\
&q_0^M=\frac{s_1+m_\pi{}^2-m_\rho{}^2}{2\sqrt{s_1}}\,,\\
&\cos\theta_1=\frac{t_1+2p_{10}^Mq_{10}^M-m_\pi{}^2-m_\rho{}^2}{2|\vec{p}_1^{\,M}||\vec{q}_1^{\,M}|}\,,\\
&\cos\psi_2=\frac{2p_{10}^Mq_{20}^M+s_1-s_{12}-t_2+m_N{}^2}{2|\vec{p}_1^{\,M}||q_2^M|}\,.
\end{aligned} \tag{3.2}$$

We denote the $s_1$-channel helicity amplitude corresponding to a $\rho$ meson with helicity $\lambda$ and momentum in the $\theta_1,\phi_1$ direction in the $M$ frame by $f_\lambda^{(s1)}(\theta_1,\phi_1,s_{12},s_1,t_2)$, or for brevity $f_\lambda^{(s1)}(\theta_1,\phi_1)$. Its decomposition in terms of partial-wave amplitudes

$F_L^{JM}$ is

$$f_\lambda^{(s_1)}(\theta_1, \phi_1) = \sum_{J,M,L} \left(\frac{2J+1}{4\pi}\right)^{1/2} D^{J*}_{M\lambda}(\phi_1, \theta_1, -\phi_1) \times \left(\frac{2L+1}{2J+1}\right)^{1/2} \langle L\,10\lambda | J\lambda\rangle\, F_L^{JM} \,. \tag{3.3}$$

In the above, $\langle L\,10\lambda|\,J\lambda\rangle$ is the Clebsch-Gordan coefficient that couples angular momenta $L$ and 1 with $z$ projections 0 and $\lambda$, respectively, to yield angular momentum $J$. Equation (3.3) may be inverted to yield

$$F_L^{JM} = \frac{1}{\sqrt{4\pi}} \int d\Omega_1 \sum_\lambda D^J_{M\lambda}(\phi_1, \theta_1, 0)(2L+1)^{1/2} \times \langle L\,10\lambda|\,J\lambda\rangle\, f_\lambda^{(s_1)}(\theta_1, \phi_1) \,. \tag{3.4}$$

We now wish to express the last result in terms of the $t_1$ channel helicity amplitudes $f_\mu^{(t_1)}(\theta_1, \phi_1)$, where $\mu$ is the helicity of the antirho in the frame where $\vec{p}_1 - \vec{q}_1 = 0$. The crossing matrix between the $s_1$-channel helicity amplitudes and the $t_1$-channel helicity amplitudes is given by

$$f_\lambda^{(s_1)}(\theta_1, \phi_1) = e^{-i\lambda\phi_1} \sum_\mu d^1_{\mu\lambda}(\omega) f_\mu^{(t_2)}(\theta_1, \phi_1) \,, \tag{3.5}$$

where

$$\cos\omega = -\frac{(m_\pi^2 - m_\rho^2 - t_2)(s_1 + m_\rho^2 - m_\pi^2) - 2m_\rho^2(2m_\pi^2 - m_\rho^2 - t_1)}{\lambda^{1/2}(s_1, m_\rho^2, m_\pi^2)\lambda^{1/2}(t_2, m_\rho^2, m_\pi^2)} \,,$$
$$\sin\omega = -(1 - \cos^2\omega)^{1/2} \,. \tag{3.6}$$

If, as mentioned before, we assume that the only nonzero $t_1$-channel amplitude is the one with $\mu = 0$, Eq. (3.4) becomes

$$F_L^{JM} = \frac{1}{\sqrt{4\pi}} \int d\Omega_1 \left\{ \sum_\lambda e^{-iM\phi_1} d^1_{0\lambda}(\omega)\, d^J_{M\lambda}(\theta_1)(2L+1)\langle L\,10\lambda|\,J\lambda\rangle \right\} f_0^{(t_1)}(\theta_1, \phi_1) \,. \tag{3.7}$$

For the amplitude $f_0^{(t_1)}(\theta_1, \phi_1)$, we shall use $A_5$, given in Eq. (2.22). We shall find it interesting to calculate the above partial waves, not only to compare with the results of previous calculations, but also to search for "Schmid loops"[13] corresponding to expected $\rho$-$\pi$ resonances.

## IV. RESULTS

In this section, we display some of the results of our calculation, and compare them with both the data and results of other calculations. For all distributions that we shall consider, the lab momentum was taken to be 25 GeV/$c$. The phase space used was subject to the cuts $|t_1| \leq 2.5$ (GeV)$^2$, $|t_2| \leq 1.0$ (GeV)$^2$. The restriction on $t_1$ was motivated by convenience; as we shall see, in our model the $t_1$ values that we omitted contribute a negligible amount to the cross section for the range of $M_{\rho\pi}$ values that we consider. The restriction on $t_2$ guarantees that for our choice of trajectories $\alpha_1$ and $\alpha_2$, and for our cutoff in $t_1$, we satisfy the condition $\alpha_1 + \alpha_2 \geq 0$, thus avoiding the singularities of the hypergeometric functions mentioned in Sec. II. As a practical matter, our calculation was insensitive to this last restriction largely due to the factors $\beta_{\pi P\pi}(t_2)$ and $\beta_{NPN}(t_2)$, which are sharply peaked in $t_2$.

In order to evaluate the performance of our model, we shall compare its predictions with data found in Ref. 2, unless otherwise stated.

The total $\rho$-$\pi$ cross section in the mass range 0.92 GeV $\leq M_{\rho\pi} \leq$ 1.5 GeV was calculated to be 139 $\mu$b. This is 44% of the observed cross section in this region, excluding the $A_2$ contribution. The calculated curve, normalized to yield the correct total cross section, is displayed as curve A in Fig. 3. We see that at large values of $M_{\rho\pi}$, the "tail" of the distribution agrees well with the data except in the vicinity of the $A_2$ and $A_3$ bumps. The peak of the distribution, occurring at $M_{\rho\pi} = 1.1$ GeV, also agrees with the data. At small values of $M_{\rho\pi}$, the leading edge of the $\rho$-$\pi$ mass distribu-

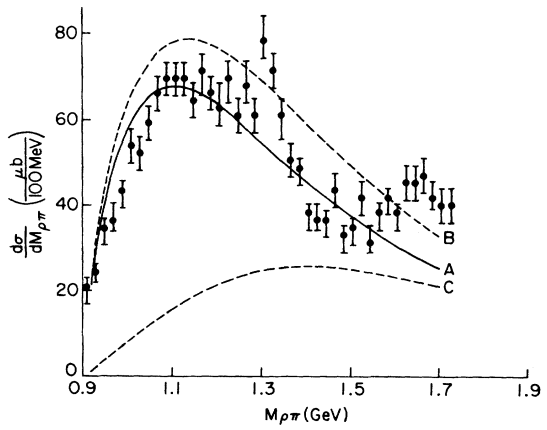


FIG. 3. Calculated $\rho\pi$ mass distribution. Curve A, full amplitude; curve B, $\pi$-$p$-cut term; curve C, $\rho$-$\pi$-cut term. Data points are from Ref. 2.

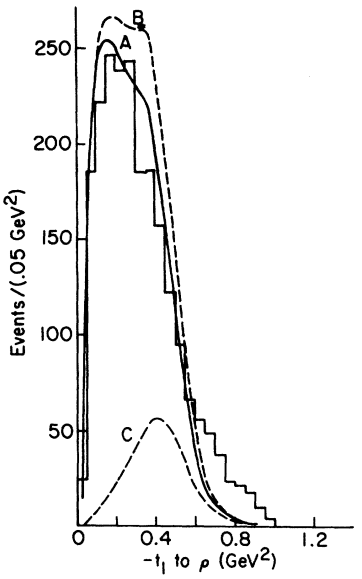


FIG. 4. Distribution in $t_1$ for 1.0 GeV $\leq M_{\rho\pi} \leq$ 1.1 GeV. Curve A, full amplitude; curve B, $\pi$-$p$-cut term; curve C, $\rho$-$\pi$-cut term. The histogram is taken from Ref. 2. Curve A is normalized to 2193 events.

tion is somewhat more rounded than the data, although not much more rounded than the calculation of Ascoli *et al.*[2] We shall speculate on the origin of this effect in Sec. V. Choices for $M(t_1, t_2)$ other than the one used tended to both broaden the distribution and reduce the total cross section.

The distribution $d\sigma/dt_2$ was calculated in the effective mass range 0.96 GeV $\leq M_{\rho\pi} \leq$ 1.2 GeV, and found to be an exponential of slope 11.66. This compares with an experimental slope[14] of 10.6 $\pm$ 2.2 at a lab momentum of 11 GeV/$c$.

In Fig. 4 we present the distribution $d\sigma/dt_1$ in the effective mass range 1.0 GeV $\leq M_{\rho\pi} \leq$ 1.1 GeV, which we compare with the 11–25 GeV/$c$ data presented in Ref. 1. Curve A, which represents the contribution of the full amplitude, reproduces the general features of the amplitude for small $|t_1|$. It is interesting to note the slight "shoulder" in the distribution at $t_1 \sim 0.42$ (GeV)$^2$. This effect is due to the fact that for small $M_{\rho\pi}$ and large $|t_1|$, we kinematically exclude forward scattered protons in the overall center of mass ($t_2 = t_{2M}$) if $s_{12}$ is held fixed. We should note, however, that we have not explicitly incorporated $\rho$-$\pi$ resonances like the $A_2$ into our model. One would expect that a strong resonance which contributes only to partial waves with small orbital angular momentum would act to broaden the tail of the distribution at large $t_1$. In curve A of Fig. 5 we see $d\sigma/dt_1$ for the effective mass range 1.5 GeV $\leq M_{\rho\pi} \leq$ 1.8 GeV. Again, we see the same kinematic "shoulder" appearing at $t_1 \sim -1.7$ (GeV)$^2$ that causes the model to drop more rapidly than the data. Again it seems reasonable

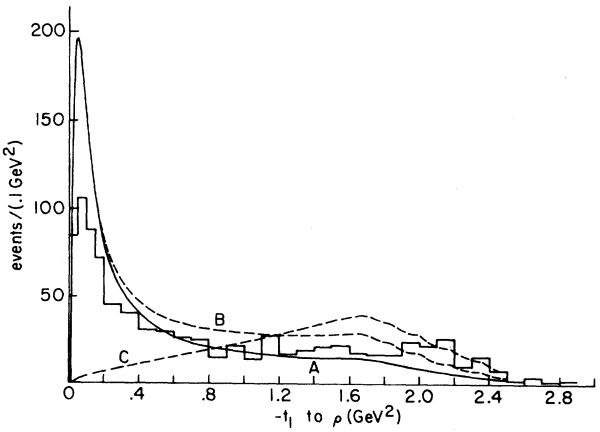


FIG. 5. Distribution in $t_1$ for 1.5 GeV $\leq M_{\rho\pi} <$ 1.8 GeV. Curve A, full amplitude; curve B, $\pi$-$p$-cut term; curve C, $\rho$-$\pi$-cut term. The histogram is taken from Ref. 2. Curve A is normalized to 694 events.

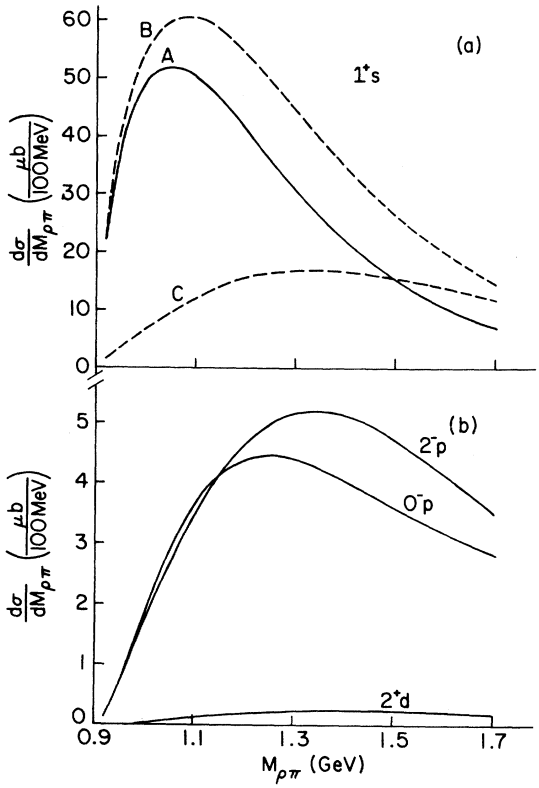


FIG. 6. Cross sections for large partial waves. (a) $1^+ s$ contribution. Curve A, full amplitude; curve B, $\pi$-$p$-cut term; curve C, $\rho$-$\pi$-cut term. (b) $2^- p$, $0^- p$, and $2^+ d$ contributions. Note the change of scale.

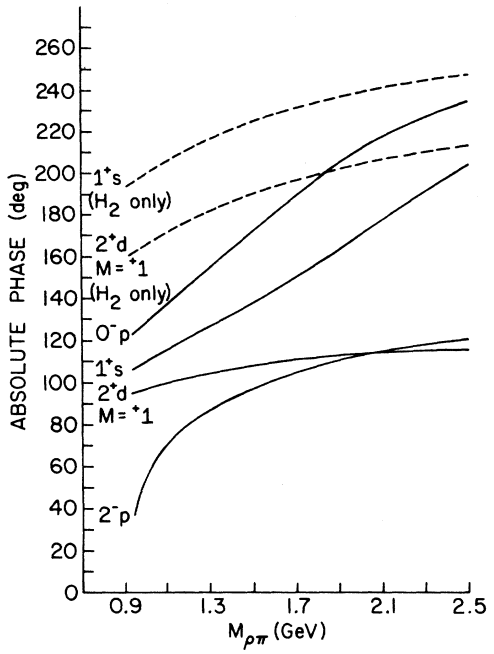


FIG. 7. Absolute phase of important partial waves as a function of $\rho$-$\pi$ mass. Unless otherwise indicated $M=0$ is shown.

that the explicit incorporation into the model of $\rho$-$\pi$ resonances would broaden the tail of the distribution. In Sec. V we shall discuss a possible program for the explicit incorporation of $\rho$-$\pi$ resonances into such a model.

In Fig. 6(a), curve A shows the contribution of the $1^+s$ partial wave to the total cross section, and in Fig. 6(b) we see the contributions of the $0^-p$, $2^-p$, and $2^+d$ partial waves. The $1^+d$ partial wave (not shown) is about $\frac{1}{4}$ as large as the $2^+d$ wave. The $1^+s$ $\rho$-$\pi$ wave, which peaks in our calculation at $M_{\rho\pi} = 1.07$ GeV, is a bit stronger than it is in the data after the amplitude has been normalized to yield the correct total cross section, as we show. This may be partly due to the fact that our curves are normalized to fit the entire three-pion data, which also contain $\epsilon$-$\pi$ final states. These states contribute strongly to the $0^-p$ wave, and their absence in our model is expected to affect adversely the ratios of the various partial wave contributions to that of the full amplitude. We do expect, however, that our model should contain the various $\rho$-$\pi$ partial waves in the same ratios as they appear in the data. This appears to be the case for the waves shown.

We now wish to examine the phases of the various partial waves. In Fig. 7, we display the absolute phases of several of the large partial waves. We notice that the relative phases compare favorably with those of Ascoli *et al.*,[1] with the exception of an abrupt increase in the phase of the $2^-p$ wave at low $M_{\rho\pi}$ values. We shall examine the origin of this effect in the next section, but first we wish to display the partial wave amplitudes in more detail.

In Figs. 8–11 we show Argand plots of the real vs the imaginary parts of the various partial waves for $t_2 = -0.05$ (GeV)$^2$. If we compare Figs. 8–10 with the corresponding plots of Ref. 1, we note the qualitative agreement between the two calculations. In Fig. 8, we see the $1^+s$ $M=0$ wave. We note that its amplitude decreases monotonically as $M_{\rho\pi}$ increases, and in addition there is a complete absence of any rapid phase variation. From our knowledge of two-body reactions, we might infer the absence of any resonant behavior in this partial wave, but as we shall see in Sec. V, this may be an oversimplification.

In Figs. 9 and 10 we see Argand plots which resemble resonant behavior in two-body reactions. In fact, by general arguments due to Schmid,[13] resonant behavior is expected in the $2^+d$ partial wave due to the $A_2$ meson; unfortunately, the

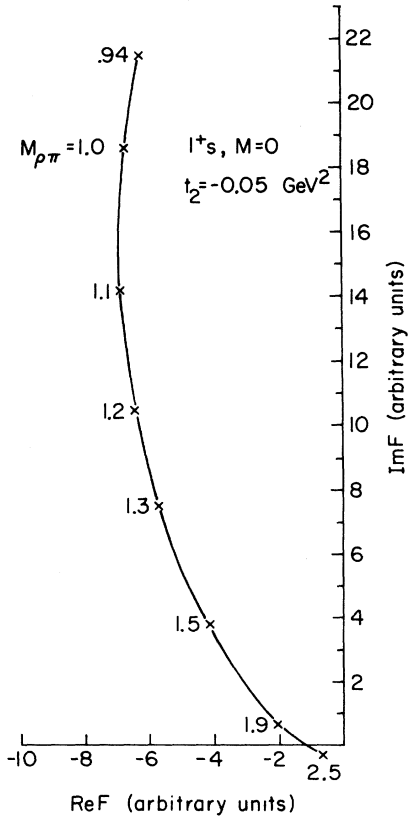


FIG. 8. Argand diagram for the $1^+s$ partial wave as a function of $M_{\rho\pi}$. $P_{\rm lab} = 25$ GeV/$c$, $t_2 = -0.05$ GeV$^2$, $M=0$.

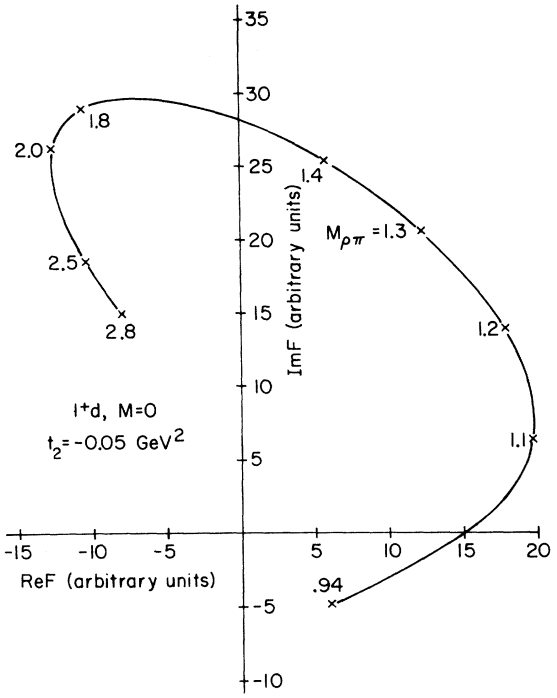


FIG. 9. Argand diagram for the $1^+d$ partial wave. $P_{\text{lab}}=25$ GeV/$c$, $t_2=-0.05$ GeV$^2$, $M=0$.

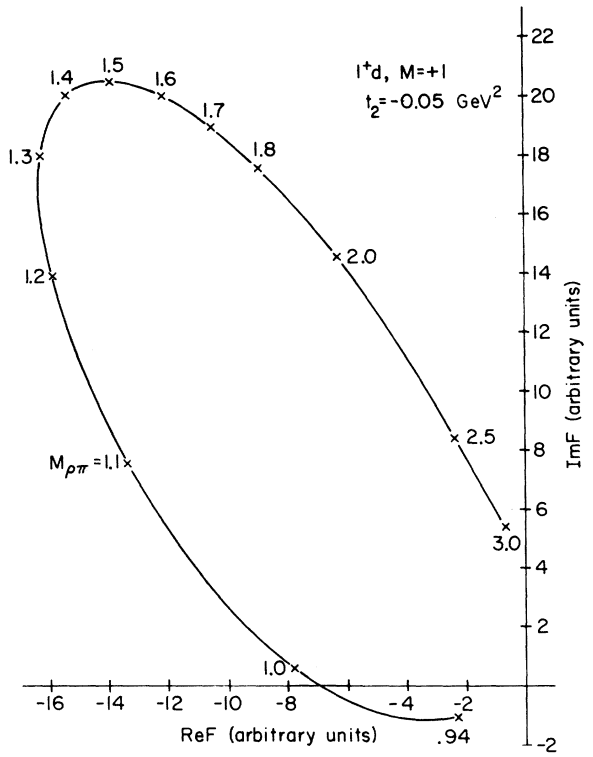


FIG. 11. Clockwise loop in the Argand diagram for the $1^+d$ partial wave. $P_{\text{lab}}=25$ GeV/$c$, $t_2=-0.05$ GeV$^2$, $M=+1$.

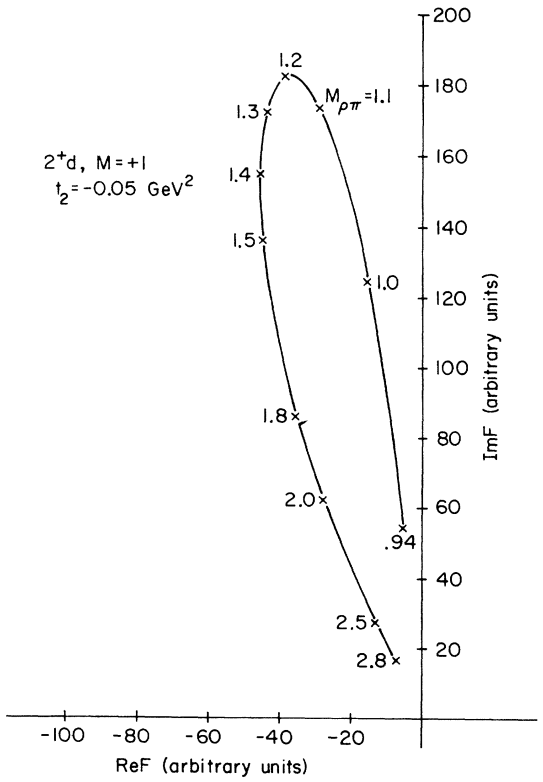


FIG. 10. Argand diagram for the $2^+d$ partial wave. $P_{\text{lab}}=25$ GeV/$c$, $t_2=-0.05$ GeV$^2$, $M=+1$.

known mass of $A_2(1.32\ \text{GeV})$ cannot be readily inferred from either the amplitude or the phase of the resulting "Schmid loop."

If we calculate other partial waves, most are seen to resemble either Fig. 9 or Fig. 10. It is interesting to note that those waves which start in the right half-plane, like the $1^+d$ wave, yield loops which tend to be full and rounded. Those which start in the left half-plane tend to be rather elongated, like the $2^+d$ wave. An extreme example of this behavior is seen in the $1^+d$ $M=+1$ wave for $t_2=-0.05$ (GeV)$^2$, shown in Fig. 11. In this example we see that the loop has been pulled inside-out and deformed into a *clockwise* loop. We shall now show that this and other surprising behavior comes about from the interplay of the two terms proportional to $V_1(t_1,t_2;\eta)$ and $V_2(t_1,t_2;\eta)$.

## V. INTERPRETATION OF THE MODEL

In light of the overall agreement between our model and the data, there are several questions that we might properly ask:

(1) Why should a Reggeized formula work so well when one of the subenergies, namely $s_1$, is barely above threshold?

(2) How can we simply interpret the rather bizarre behavior of the Schmid loops and perhaps relate it in a more obvious fashion with the known $\rho$-$\pi$ resonances?

(3) Why is no Schmid loop seen in the $1^+s$ wave?

In order to answer the above questions, we first return to Eq. (2.22), which we now write in the form

$$A_5 = H_1 + H_2 , \tag{5.1}$$

where

$$H_1 = \beta_1(t_1)\beta_2(t_2)\Gamma(-\alpha_1)\Gamma(-\alpha_2) s_2^{\alpha_2-\alpha_1} s_{12}^{\alpha_1} \times \xi_1\xi_{21} V_1(t_1, t_2; \eta) , \tag{5.2}$$

$$H_2 = \beta_1(t_1)\beta_2(t_2)\Gamma(-\alpha_1)\Gamma(-\alpha_2) s_1^{\alpha_1-\alpha_2} s_{12}^{\alpha_2} \times \xi_2\xi_{12} V_2(t_1, t_2; \eta) . \tag{5.3}$$

As we see from Eqs. (2.26) and (2.27), $V_1$ and $V_2$ have spurious poles for those values of $t_1$ and $t_2$ such that $|\alpha_1 - \alpha_2|$ is an integer, although these poles cancel in the signatured amplitude $A_5^{\tau_1\tau_2}$. We notice though, that since $\alpha_1 > -1$ for our Pignotti-type trajectory, the condition $\alpha_1 + \alpha_2 > 0$ implies that $|\alpha_1 - \alpha_2| < 2$ in the physical region of our reaction. As a result, the only spurious poles that we encounter occur for $|\alpha_1 - \alpha_2| = 1$. This is fortunate, since at these points $\xi_{12} = \xi_{21} = 0$, and $H_1$ and $H_2$ each separately remain finite. We yield to the obvious temptation to calculate the contributions of the separate terms to the cross section, and we show the results in Fig. 3.

Curve B of Fig. 3 shows that the dominant contribution to the $\rho$-$\pi$ mass spectrum in the $A_1$ region comes from the term $H_1$. This is an interesting fact, since $H_1$ has the asymptotic behavior $s_2^{\alpha_2-\alpha_1} s_{12}^{\alpha_1}$. In the $A_1$ region, both $s_2$ and $s_{12}$ are large; hence we see that the dominant term is in its asymptotic region. We see from curve C that the term $H_2$, which has the asymptotic behavior $s_1^{\alpha_1-\alpha_2} s_{12}^{\alpha_2}$, is small in the $A_1$ region. This too, is noteworthy, since $s_1$ is barely above threshold. We can conclude that, at least within the framework of this model, Reggeization is a reasonable procedure since the dominant term which contributes to the cross section is in its Regge limit. This last conclusion is not at all obvious in a "naive" Reggeization as in Ref. 2.

In order to obtain a possible interpretation of the physical significance of the terms $H_1$ and $H_2$, it is useful to examine their separate contributions to $d\sigma/dt_1$, shown in Figs. 4 and 5. We see in both graphs that the $H_1$ contribution, again given by curve B, contains a sharp spike in the small-$t_1$ region, while the $H_2$ distribution (curve C) is much broader. This shows that $H_2$ mainly receives contributions from the small-$J$ partial waves, while

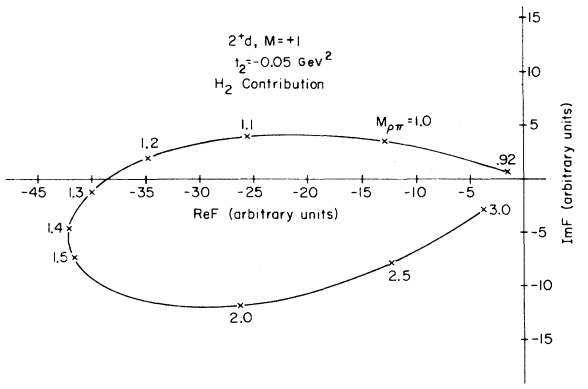


FIG. 12. Schmid loop from the $H_2$ contribution to the $2^+d$ $M=+1$ partial wave. $P_{lab}=25$ GeV/$c$, $t_2=-0.05$ GeV$^2$. Units are the same as in Fig. 10.

$H_1$ receives a significant contribution from the higher-$J$ partial waves. Since $H_2$ has a nonzero discontinuity in the subenergy $s_1$ as a Feynman diagram containing a $\rho$-$\pi$ resonance would, it is inviting to regard $H_2$ as containing a "dual average" to the $\rho$-$\pi$ resonances. From Fig. 3 then, we see that the main contribution to the cross section comes from the "nonresonant" piece $H_1$.

If $H_2$ were to contain most or all of the contribution of the $\rho$-$\pi$ resonances it would be interesting to partial-wave-analyze this term alone. Since $\alpha_1 > -1$, we may substitute $H_2$ into Eq. (3.7), and the angular integrals will not violate the condition $\alpha_1 + \alpha_2 > 0$ if $|t_2|$ is sufficiently small. In Figs. 12 and 13 we see the results of such an analysis on the $2^+d$ partial waves. Both curves clearly resemble resonance loops, and the $M=+2$ partial wave peaks very near the $A_2$ mass. The $H_1$ contribution is almost purely positive imaginary, first increasing at the $\rho\pi$ threshold, then gradually decreasing for large $M_{\rho\pi}$. It turns out that resonancelike loops are seen

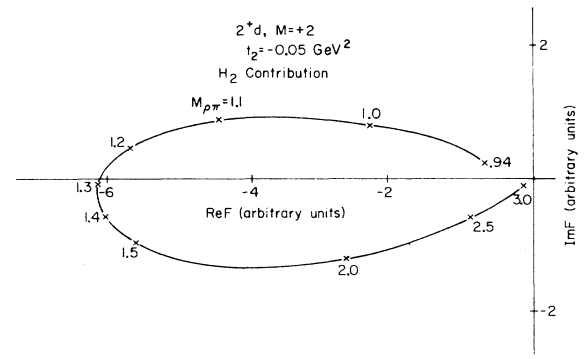


FIG. 13. Schmid loop from the $H_2$ contribution to the $2^+d$ $M=+2$ partial wave. $P_{lab}=25$ GeV/$c$, $t_2=-0.05$ GeV$^2$. Units are the same as in Fig. 10.

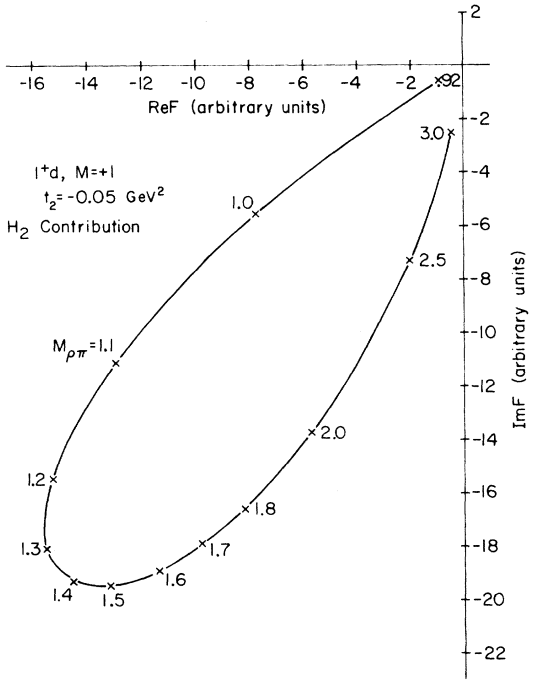


FIG. 14. Schmid loop from the $H_2$ contribution to the $1^+d$ $M=+1$ partial wave. $P_{\text{lab}}=25$ GeV/$c$, $t_2=-0.05$ GeV$^2$. Units are the same as in Fig. 9.

in the $H_2$ contribution to all of the partial waves. We should not take this model's predictions of resonances too seriously then, but we can gain some insight into the behavior of the partial waves, if resonances actually were present.

We may readily understand the rapid increase in phase that some of the partial waves display just above the $\rho$-$\pi$ threshold. If we partial-wave-analyze the $H_2$ contribution to these partial waves, we obtain loops like those shown in Figs. 12 and 13, but rotated clockwise by 90°. Thus for low $M_{\rho\pi}$, both the $H_1$ and $H_2$ contributions are increasing in the $+i$ direction, and the resultant sum varies rapidly in phase. In cases such as these (the $1^+d$ $M=0$ partial wave shown in Fig. 9, and the $2^-p$ $M=0$ wave with phase displayed in Fig. 7) the initial rapid increase in phase is not due to resonant behavior, but rather to the phase relation between $H_1$ and $H_2$. In general, those partial waves ($M \geq 0$) that start in the right half-plane form rounded loops with a rapid increase in phase at low $M_{\rho\pi}$.

The rather "flattened" loops, such as those occurring in the $2^+d$ waves, result from the fact that the contributions from $H_1$ and $H_2$ do not initially increase in the same direction. These waves start in the left half-plane, and their $H_2$ contributions, which are again counterclockwise loops, tend to move in the $-i$ direction, while the $H_1$ contribution, as before, moves in almost exactly the $+i$ direction. Another example of this is shown in Fig. 14, which displays the $H_2$ contribution to the $1^+d$ $M=+1$ partial wave. Again, we have a counterclockwise loop. As we saw in Fig. 11, however, when we add this piece to the $H_1$ contribution (which has an almost purely imaginary, and therefore stationary, phase) we obtain a clockwise loop.

In light of the above discussion, we conclude that if the $\rho$-$\pi$ resonances contribute to the $H_2$ term, they can only be seen if either the resonance contribution is very strong, or else the $H_1$ contribution is very small. It seems reasonable that the $A_2$ has been seen in this reaction partly because of the $d$-wave threshold behavior of the $H_1$ contribution to the $2^+d$ partial wave.

Finally, we may ask whether this resonancelike behavior is present in the partial wave amplitude for the $1^+s$ wave. In Fig. 15, we see the $H_2$ contribution to the $1^+s$ $M=0$ partial wave. Again we see a Schmid loop corresponding to resonancelike behavior. It is interesting to note that the mass of the "resonance" is about 1.1 GeV. Apparently, the $H_1$ contribution is large at the $\rho$-$\pi$ threshold due to the absence of kinematic threshold factors in this partial wave. This "nonresonant" term acts as a background that masks any resonant behavior that may actually be present.

It is interesting to speculate on the existence of an $A_1$ "resonance," and the possibility of incorporating it, along with other $\rho$-$\pi$ resonances such as the $A_2$, into the model. As we have seen, the term $H_2$ contains Schmid loops corresponding to $\rho$-$\pi$ resonances, while the $H_1$ term contributes a piece with nonrotating phase to the partial waves. It seems reasonable, then, that we could replace the $H_2$ term with several tree graphs corresponding to $\rho$-$\pi$ resonances like the $A_2$ and (hypothetical) $A_1$. More sophisticated approaches may read-

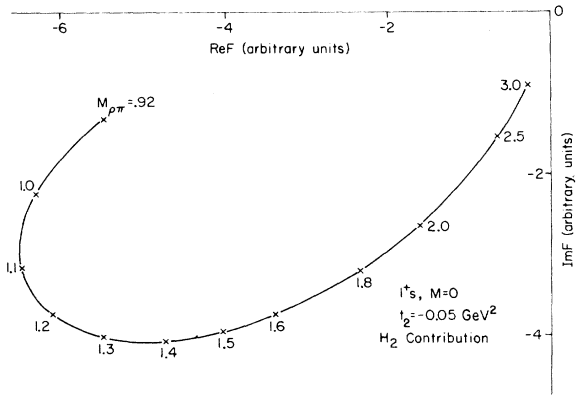


FIG. 15. Schmid loop from the $H_2$ contribution to the $1^+s$ $M=0$ partial wave. $P_{\text{lab}}=25$ GeV/$c$, $t_2=-0.05$ GeV$^2$. Units are the same as in Fig. 8.

ily be imagined, and this general type of approach would not involve any double-counting of the resonances if we were to retain the $H_1$ term, since that term does not appear to have much (if any) resonance content. If we look at Figs. 3 and 6(a), we see that an $A_1$ "resonance" at about 1.15 GeV would contribute negligibly to the leading edge of the $\rho$-$\pi$ mass spectrum. The resultant curve would more nearly resemble B in shape in this region; this is desirable since curve B is more sharply peaked, and hence bears a greater resemblance to the data. The addition of a term corresponding to an $A_2$ resonance would not affect the mass spectrum in regions far from the $A_2$ mass, since as we see in Fig. 6(b), the $2^+d$ wave is relatively small in our calculation.

## VI. SUMMARY

We conclude that the reaction $\pi^- p \to \rho^0 \pi^- p$ can be described by a double-Regge amplitude that does not contain simultaneous discontinuities in $s_1$ and $s_2$ when the amplitude is evaluated in the double-Regge limit. The shape of the calculated $3\pi$ mass distribution agrees with the data. The main contribution to the mass spectrum comes from the term $H_1$, which we interpret as being nonresonant. The slightly improved width of the distribution is due partly to the interference of $H_1$ with the term $H_2$, which we interpret to contain the $\rho$-$\pi$ resonances.

We obtain partial-wave amplitudes that agree with the calculations of Ascoli *et al.* In the $1^+s$ partial wave, the resonancelike contribution of $H_2$ is hidden by the $H_1$ contribution. This effect is particularly strong in this partial wave due to the phase relation of the two terms and the absence of threshold suppression factors.

Finally, the success of this model is readily understood by noting that the dominant term $H_1$ has the asymptotic behavior $s_2^{\alpha_2-\alpha_1} s_{12}^{\alpha_1}$. In the "$A_1$" region of phase space, this term approaches its asymptotic limit; the success of Reggeization is then not unexpected.

As a closing comment we speculate on the possible existence of an $A_1$ meson. As we have noted, the $H_2$ contribution to *all* of the partial-wave amplitudes contains Schmid loops, so that a Schmid loop in the $1^+s$ wave can hardly be considered "proof" of the existence of such a resonant state. However, the facts that the Argand plot of the $H_2$ contribution peaked at about 1.1. GeV (in the middle of the high "nonresonant" $3\pi$ bump) and that the large "nonresonant" term ($H_1$) tends to dominate the $1^+s$ partial wave, suggest that perhaps the (exclusive) final state $\pi^+\pi^-\pi^- p$ is a poor choice in which to search for the $A_1$. One might hope that these detrimental effects could be minimized, for example in inclusive $3\pi$ production, so that more definitive results could be obtained.

## ACKNOWLEDGMENTS

The author wishes to express his deep appreciation to Professor Lorella M. Jones for suggesting the problem, and for countless hours of valuable discussion. He also wishes to thank W. W. MacKay and C. W. Wingate for important computational assistance. Finally, he wishes to thank the Illinois High Energy Experimental Group for the use of their computer facility. This research was supported in part by NSF Grant No. PHYS 75-21590.

[1]G. Ascoli *et al.*, Phys. Rev. D 8, 3894 (1973).
[2]G. Ascoli *et al.*, Phys. Rev. D 9, 1963 (1974).
[3]O. Steinmann, Helv. Phys. Acta. 33, 275 (1960); 33, 347 (1960).
[4]H. Araki, J. Math. Phys. 2, 163 (1961).
[5]K. E. Cahill and H. P. Stapp, Phys. Rev. D 8, 2714 (1973).
[6]L. M. Jones, Phys. Rev. D 14, 3233 (1976).
[7]J. H. Weis, Phys. Rev. D 6, 2823 (1972).
[8]C. D. Froggatt and G. Ranft, Phys. Rev. Lett. 23, 943 (1969).
[9]R. C. Brower, C. E. DeTar, and J. H. Weis, Phys. Rep. 14C, 259 (1974).
[10]I. T. Drummond, P. V. Landshoff, and W. J. Zakrzewski, Phys. Lett. 28B, 676 (1969).
[11]E. L. Berger, Phys. Rev. 166, 1525 (1968).
[12]A. R. White, Nucl. Phys. B67, 189 (1973).
[13]C. Schmid, Phys. Rev. Lett. 20, 689 (1968); Nuovo Cimento 61A, 289 (1969).
[14]G. Caso *et al.*, Nuovo Cimento 47, 675 (1967).